This paper appears in The International Journal of Medical Robotics and Computer Assisted Surgery, 2018.
https://doi.org/10.1002/rcs.1900

Towards Robot-Assisted Anchor Deployment in Beating-Heart Mitral Valve Surgery

Lingbo Cheng, Mojtaba Sharifi, and Mahdi Tavakoli*

ABSTRACT

Background: Beating-heart intracardiac surgery promises significant benefits for patients compared to cardiopulmonary bypass based procedures. However, the fast motions of the heart introduce serious challenges for surgeons.

Methods: In this paper, a new impedance-controlled master-slave telerobotic system is developed to help perform anchor deployment for mitral valve annuloplasty under the guidance of live ultrasound images of the heart. The proposed bilateral teleoperation system can both reflect the non-oscillatory portion of slave-heart tissue interaction force on the surgeon's hand as haptic feedback and implement rapid compensation for the beating heart's motion. The surgical task involves performing anchor deployment on a simulated moving heart tissue to evaluate the effectiveness of the proposed strategy for safely interacting with a moving organ.

Results and Conclusions: The obtained results show that the telerobotic system increases the success rate of anchor deployment by 100% and reduces the excess force application rate by 70% compared to manual attempts.

KEYWORDS

Robot-assisted surgery, telerobotics, impedance control, beating-heart surgery, mitral valve annuloplasty

1. INTRODUCTION

In recent years, robotic systems have been employed for surgery, where a surgeon interacts with a master robot to perform a desired task on the target tissue by a surgical tool mounted on a slave robot [1], [2]. These systems can be used to perform extra- and intra-cardiac surgeries while the heart is arrested [3]. However, arrested-heart surgery has adverse effects due to using cardiopulmonary bypass (CPB) [4-8]. There is a major source of morbidity following CPB, which is the systemic inflammatory response associated with increased cytokine production and complement activation that can result in neurologic dysfunction in adults and neurodevelopmental dysfunction in children [6-8]. Beating-heart surgery could eliminate such negative effects of CPB by allowing the heart to beat normally [9], and also enables intraoperative evaluation of the heart tissue motion, which is critical to the assessment of reconstructive heart operations, particularly for mitral valve surgery [10]. However, beating-heart surgery is challenging due to the need for heart tissue motion compensation during the surgical operation in order to minimize the risks of tool-tissue collision and tissue injury. If a robotic system could move a surgical tool in synchrony with the target tissue while the heart beats, the surgeon could then perform the surgical procedure as if the beating heart were stationary.

Several position-based motion compensation methods have been proposed in the literature for enabling beating-heart surgery. Nakamura et al. using a 4 degree-of-freedom (DOF) robot guided by two high-speed cameras demonstrated automatic tracking of a point on the heart that was lit by laser [11]. Ginhoux et al [12] proposed using a 6-DOF AESOP robot guided by a high-speed camera to track LEDs attached to a beating porcine heart. These sensors provided real-time and accurate position information to compensate for the rapid movement of the beating heart. However, high-speed cameras can only visualize the outer surface of the heart, and are not appropriate for surgeries performed inside the heart such as mitral valve repairs.

In this work, ultrasound machine is used for guiding intracardiac beating heart repairs as it can provide tissue images through blood. In previous work [13-15], our group used ultrasound images and combined it with a Smith

predictor and a generalized predictive controller, respectively, to estimate and compensate for the beating heart's motion. The acquisition and processing of ultrasound images cause a large time delay, which need to be compensated for via control. To avoid this non-negligible time delay, in this paper, we presented a new impedance-controlled master-slave telerobotic system for beating heart surgery while the surgeon guides the surgical tool under live ultrasound images. And then we validated the system's performance in a specific simulated surgical task — mitral valve annuloplasty.

Every year, 300,000 people worldwide undergo open heart surgery for mitral valve repair [16]. When the two leaflets normally involved in sealing the mitral valve do not coaptate properly, a reconstructive procedure called mitral valve annuloplasty may be used to address this problem. This surgery involves implanting an annuloplasty ring onto the mitral valve using several anchors; pulling a string that goes through the ring pulls the leaflets together to facilitate coaptation and aid to reshape the mitral valve [17], [18], and it has better durability and reliability than ringless repairs, except recurrent regurgitation not resulting in reoperation may occur [19]. To enable the performing of this particular surgical task when the heart is beating, a motion compensation system is needed. The instruments used for mitral valve annuloplasty involve two parts (Fig. 1). One instrument is the annuloplasty ring holder. The other one is the anchor driver mounted on the end of the slave robot. The anchor driver is a thin rigid tube and deploys anchors that secure the stiff ring to the annulus to reshape it. To reach the interior heart tissue, both of the instruments are inserted into the left atrium through a suture on the exterior heart wall [20]. In the experiments, for the sake of brevity, we simulated the procedure of anchor deployment using a phantom tissue that undergoes movements similar to that of a beating heart. In the following, a detailed description of the proposed strategy is presented, and then an evaluation in terms of safely interacting with a moving organ is implemented in a water tank.

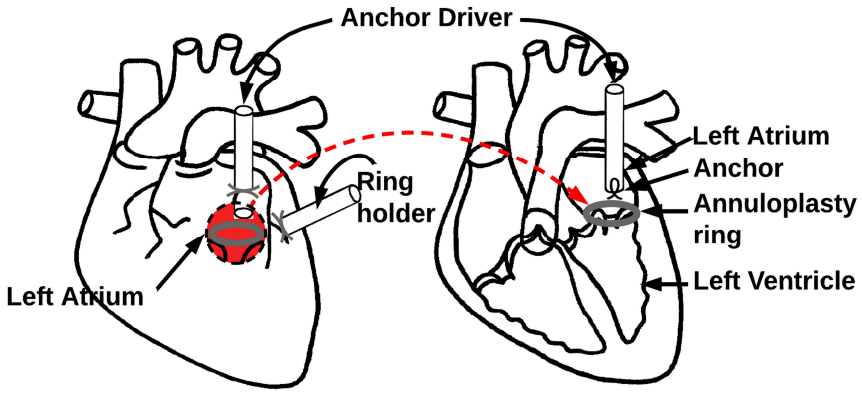

Fig.1. Diagram of proposed mitral valve annuloplasty procedure.

2. MATERIALS AND METHODS

To enable the performing of anchor deployment when the heart is beating, a motion compensation system such as the one shown in Fig. 2 is needed. To begin, the surgeon should use one of his/her hands to control a telerobotic system, which includes a master and a slave robot to bring an anchor driver attached to the end-effector of slave robot close to the beating-heart tissue. Once the anchor driver and the heart tissue contact, the surgeon could use his/her other hand to execute the anchor deployment. All of these are guided by ultrasound images provided to the surgeon. In this paper, two bilateral impedance controllers are designed for the master and slave robots to compensate for the beating-heart's motion so as to improve the success rate of deploying anchors and minimize the risk of tool-tissue collision and tissue injury.

The two desirable objectives of the proposed bilateral teleoperation system are (I) reflecting the non-oscillatory slave-heart tissue interaction force on the surgeon's hand as relatively steady haptic feedback, and (II) rapid compensation for the beating heart's motion so that the distance between the surgical tool and the heart tissue can be

controlled by the surgeon (i.e., the tool-tissue distance is kept fixed through feedback control until and unless the surgeon's hand moves). These behaviors can be achieved via appropriately adjusting the parameters of the two reference impedance models for the master and slave robots.

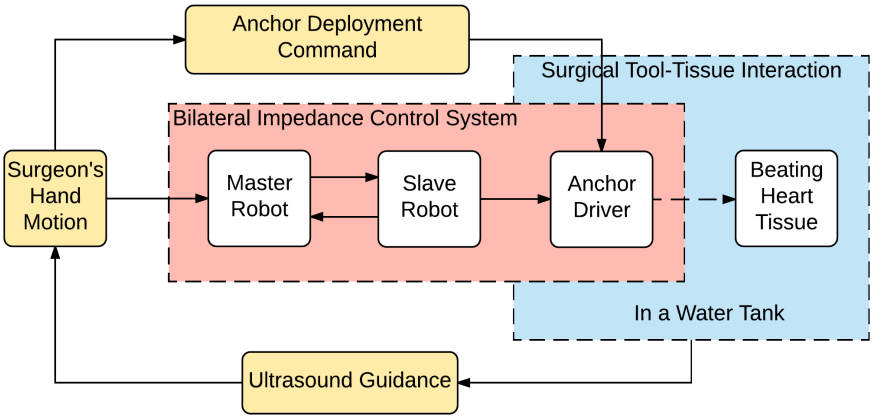

Fig.2. Motion compensation system.

2.1. Telerobotic system

This section presents two reference impedance models for slave and master robots, respectively. The reference impedance models of the master and slave robots are both defined as dynamical relationships (Fig. 3).

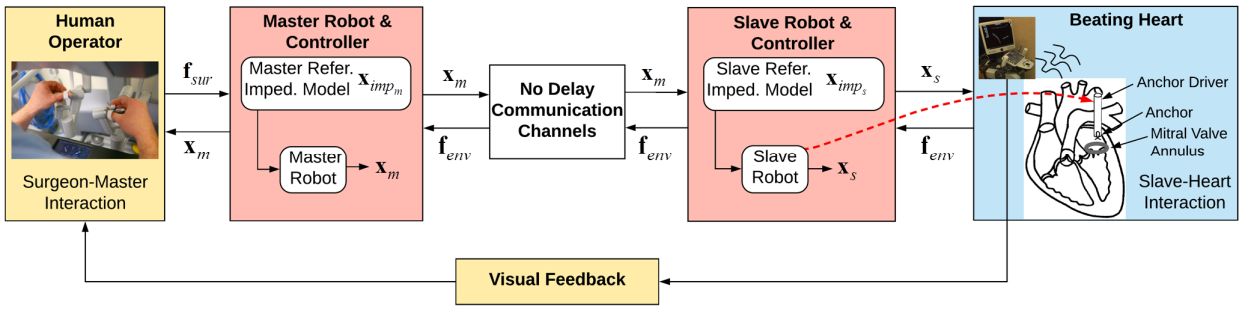

Fig.3. The concepts of master and slave reference impedance models in the proposed bilateral controller for robotic surgery systems.

The former model takes the summation of the surgeon and scaled heart tissue forces and desired master response trajectory into consideration. The latter model is concerned with the slave-heart tissue interaction force and the desired slave impedance model's response deviation from the master trajectory. Both of the trajectories are in Cartesian coordinates. The relationships can be expressed as:

$$m_m \ddot{\mathbf{x}}_{imp_m} + c_m \dot{\mathbf{x}}_{imp_m} + k_m \mathbf{x}_{imp_m} = \mathbf{f}_{sur} - k_f \mathbf{f}_{env} \tag{1}$$

$$m_s \ddot{\tilde{\mathbf{x}}}_{imp_s} + c_s \dot{\tilde{\mathbf{x}}}_{imp_s} + k_s \tilde{\mathbf{x}}_{imp_s} = -\mathbf{f}_{env} \tag{2}$$

where $\mathbf{x}_{imp_m}$ and $\mathbf{x}_{imp_s}$ are the positions of the master and slave impedance models, respectively. $\tilde{\mathbf{x}}_{imp_s} = \mathbf{x}_{imp_s} - k_p \mathbf{x}_m$, here k_p is the position scaling factor, $\mathbf{x}_m \in \mathbb{R}^{6\times1}$ is the Cartesian position of the master robot's end-effector. k_s, c_s, m_s and k_m, c_m, m_m are the virtual stiffness, damping and mass parameters of the slave and master impedance models, respectively. $\mathbf{f}_{env} \in \mathbb{R}^{6\times1}$ is the interaction force that the environment (heart tissue) applies

to the slave robot, $\mathbf{f}_{sur} \in \mathbb{R}^{6\times1}$ is the interaction force that the surgeon applies to the master robot, and k_{f} is the force scaling factor.

The reference impedance models for slave and master robots are stable second-order differential equations when the impedance parameters are set as positive. In order to make the telerobotic system have motion compensation for the fast beating heart's motion, the most crucial procedure is parameter adjustment for the two reference impedance models for the master and slave robots.

The master impedance model (1) should be designed to provide feedback of the non-oscillatory part of the slave-heart tissue interaction force for the surgeon and not to reflect the oscillatory motion to the surgeon's hand so that to avoid fatigue and exhaustion, which means $(\mathbf{f}_{sur} - k_{\mathrm{f}}\mathbf{f}_{env}) \to 0$ when the high frequency of the slave/heart interaction force ($\mathbf{f}_{env}$) has been filtered. To achieve this static force reflecting performance, the stiffness parameter, k_m, of the master impedance model should be chosen small, and the natural frequency of the master impedance model should be much lower than that of the beating heart ω_{n_H} which has a range of $6.28 \sim 10.68\,\mathrm{rad/sec}$, that is $\omega_{n_m} = \sqrt{k_m / m_m}$ should have a low natural frequency ($\omega_{n_m} \le 0.6\mathrm{rad/sec} \ll \omega_{n_H}$) [21]. In addition, in order to get a fast behavior in response to the harmonic physiological force of the surgeon, the damping ratio of the master impedance model is chosen to be $\zeta_m = c_m / 2\sqrt{m_m k_m} = 0.7$.

The slave impedance model (2) should be adjusted such that the slave robot complies with the physiological force and/or the disturbance of beating heart during the procedure of tracking the scaled master robot's trajectory, that is the flexibility of the slave robot is the deviation from the master trajectory ($\tilde{\mathbf{x}}_{imp_s} = \mathbf{x}_{imp_s} - k_{\mathrm{p}}\mathbf{x}_m$) based on the magnitude of the slave/heart interaction force ($\mathbf{f}_{env}$). It should be noticed that the values of the slave impedance parameters can neither be too small nor too large, because too small values will lead to a super flexible slave robot that it cannot apply enough forces to the heart and too large values will make the slave robot very rigid that the motion compensation will not be accurate. Therefore, the stiffness value of the slave impedance model (k_s) should be adjusted to be moderate.

Similarly, to get a fast behavior in response to the harmonic physiological force of the heart, the damping ratio of the slave impedance model is chosen to be $\zeta_s = c_s / 2\sqrt{m_s k_s} = 0.7$. The natural frequency of the impedance model should be greater than the frequency of the beating heart, that is $\omega_{n_s} = \sqrt{k_s / m_s}$ should have a high natural frequency ($\omega_{n_s} \ge 35\mathrm{rad/sec} \gg \omega_{n_H}$) [21]. For these purposes, the adjusted parameters of the two impedance models are listed in TABLE 1.

TABLE 1 ADJUSTMENT OF SLAVE AND MASTER IMPEDANCE MODELS FOR ROBOTIC SURGERY OF BEATING HEART

CHARACTERISTIC	Master Impedance Adjustment	Slave Impedance Adjustment
Stiffness	$k_m = 5$ N/m	$k_s = 100$ N/m
Damping Ratio	$\zeta_m = 0.7$	$\zeta_s = 0.7$
Natural Frequency	$\omega_{n_m} = 0.5$rad/sec	$\omega_{n_s} = 50$rad/sec
Damping and Mass	$m_m = 20$, $c_m = 14$	$m_s = 0.04$, $c_s = 2.8$
Scaling Factor	$k_{\mathrm{f}} = 1$	$k_{\mathrm{p}} = 1$

2.2. Nonlinear Bilateral Adaptive Impedance Controller

In a nonlinear master-slave teleoperation system with master position $\mathbf{x}_m$ and slave position $\mathbf{x}_s$, the dynamics of the master and slave in the Cartesian space are [22]

$$\mathbf{M}_{\mathbf{x},m}(\boldsymbol{\theta}_m)\ddot{\mathbf{x}}_m + \mathbf{C}_{\mathbf{x},m}(\boldsymbol{\theta}_m,\dot{\boldsymbol{\theta}}_m)\dot{\mathbf{x}}_m + \mathbf{G}_{\mathbf{x},m}(\boldsymbol{\theta}_m) + \mathbf{F}_{\mathbf{x},m}(\dot{\boldsymbol{\theta}}_m) = \mathbf{f}_{sur} + \mathbf{f}_m \tag{3}$$

$$\mathbf{M}_{\mathbf{x},s}(\boldsymbol{\theta}_s)\ddot{\mathbf{x}}_s + \mathbf{C}_{\mathbf{x},s}(\boldsymbol{\theta}_s,\dot{\boldsymbol{\theta}}_s)\dot{\mathbf{x}}_s + \mathbf{G}_{\mathbf{x},s}(\boldsymbol{\theta}_s) + \mathbf{F}_{\mathbf{x},s}(\dot{\boldsymbol{\theta}}_s) = \mathbf{f}_s - \mathbf{f}_{env} \tag{4}$$

where $\boldsymbol{\theta}_i$ is the joint angle of the robot's end-effector, $\mathbf{f}_i$ is the control torque of the robot, and $\mathbf{M}_{\mathbf{x},i}(\boldsymbol{\theta}_i)$, $\mathbf{C}_{\mathbf{x},i}(\boldsymbol{\theta}_i,\dot{\boldsymbol{\theta}}_i)$, $\mathbf{G}_{\mathbf{x},i}(\boldsymbol{\theta}_i)$ and $\mathbf{F}_{\mathbf{x},i}(\dot{\boldsymbol{\theta}}_i)$ are the inertia matrix, the centrifugal and Coriolis term, the gravity term, and the friction torque, respectively. Note that $i = m$ for the master and $i = s$ for the slave.

The kinematic transformations between the Cartesian space and the joint space are expressed as

$$\mathbf{x}_i = \boldsymbol{\Omega}_i(\boldsymbol{\theta}_i),\ \dot{\mathbf{x}}_i = \mathbf{J}_i(\boldsymbol{\theta}_i)\dot{\boldsymbol{\theta}}_i,\ \ddot{\mathbf{x}}_i = \mathbf{J}_i(\boldsymbol{\theta}_i)\ddot{\boldsymbol{\theta}}_i + \dot{\mathbf{J}}_i(\boldsymbol{\theta}_i)\dot{\boldsymbol{\theta}}_i \tag{5}$$

where $\mathbf{J}_i(\boldsymbol{\theta}_i) = d\boldsymbol{\Omega}_i(\boldsymbol{\theta}_i)/\mathrm{d}\,\boldsymbol{\theta}_i$ is the Jacobian matrix.

The matrices have the following properties [23]:

Property 1. The matrix $\mathbf{M}_{\mathbf{x},i}(\boldsymbol{\theta}_i)$ is symmetric and positive definite.

Property 2. $\dot{\mathbf{M}}_{\mathbf{x},i}(\boldsymbol{\theta}_i) - 2\mathbf{C}_{\mathbf{x},i}(\boldsymbol{\theta}_i,\dot{\boldsymbol{\theta}}_i)$ is skew symmetric.

Property 3. The left hand of (3) and (4) can be linearly parameterized as

$$\mathbf{M}_{\mathbf{x},i}(\boldsymbol{\theta}_i)\boldsymbol{\Psi}_{1,i} + \mathbf{C}_{\mathbf{x},i}(\boldsymbol{\theta}_i,\dot{\boldsymbol{\theta}}_i)\boldsymbol{\Psi}_{2,i} + \mathbf{G}_{\mathbf{x},i}(\boldsymbol{\theta}_i) + \mathbf{F}_{\mathbf{x},i}(\dot{\boldsymbol{\theta}}_i) = \mathbf{Y}_{\mathbf{x},i}(\boldsymbol{\Psi}_{1,i},\boldsymbol{\Psi}_{2,i},\boldsymbol{\theta}_i,\dot{\boldsymbol{\theta}}_i)\hat{\boldsymbol{\theta}}_{\mathbf{x},i} \tag{6}$$

where $\hat{\boldsymbol{\theta}}_{\mathbf{x},i}$ is the vector of unknown parameters of the robot, and the regressor matrix $\mathbf{Y}_{\mathbf{x},i}$ contains known functions in the Cartesian space. The known vectors $\boldsymbol{\Psi}_{1,i}$ and $\boldsymbol{\Psi}_{2,i}$ are chosen according to the application.

In order to realize the responses tracking of the above two reference impedance models for the master and slave robots respectively, two nonlinear bilateral adaptive impedance control laws [21, 24] in Cartesian space are designed and expressed as:

$$\mathbf{f}_m = -\lambda_{1,m}\hat{\mathbf{M}}_{\mathbf{x},m}\mathbf{s}_m + \hat{\mathbf{M}}_{\mathbf{x},m}\ddot{\mathbf{x}}_{r,m} + \hat{\mathbf{C}}_{\mathbf{x},m}\dot{\mathbf{x}}_{r,m} + \hat{\mathbf{G}}_{\mathbf{x},m} + \hat{\mathbf{F}}_{\mathbf{x},m} - \mathbf{f}_{sur} \tag{7}$$

$$\mathbf{f}_s = -\lambda_{1,s}\hat{\mathbf{M}}_{\mathbf{x},s}\mathbf{s}_s + \hat{\mathbf{M}}_{\mathbf{x},s}\ddot{\mathbf{x}}_{r,s} + \hat{\mathbf{C}}_{\mathbf{x},s}\dot{\mathbf{x}}_{r,s} + \hat{\mathbf{G}}_{\mathbf{x},s} + \hat{\mathbf{F}}_{\mathbf{x},s} + \mathbf{f}_{env} \tag{8}$$

where $\mathbf{s}_i = \dot{\tilde{\mathbf{x}}}_i + \lambda_{2,i}\tilde{\mathbf{x}}_i$ is the designed sliding surface, $\dot{\mathbf{x}}_{r,i} = \dot{\mathbf{x}}_{imp_i} - \lambda_{2,i}\tilde{\mathbf{x}}_i$ is defined as the reference velocity for the robot, $\tilde{\mathbf{x}}_i = \mathbf{x}_i - \mathbf{x}_{imp_i}$ is the position tracking error of the robot. $\lambda_{1,i}$ and $\lambda_{2,i}$ are positive constant parameters guarantee the stability of sliding surfaces (i.e. $\tilde{\mathbf{x}}_i \to 0$ as $\mathbf{s}_i \to 0$). The accent $\wedge$ denotes the estimated and updated values of matrices, vectors and scalars. $\hat{\mathbf{M}}_{\mathbf{x},i}$, $\hat{\mathbf{C}}_{\mathbf{x},i}$, $\hat{\mathbf{G}}_{\mathbf{x},i}$ and $\hat{\mathbf{F}}_{\mathbf{x},i}$ are the estimated inertia matrix, Coriolis and centrifugal vector, gravity vector and friction vector, respectively. Also, based on (2), $\mathbf{x}_{imp_s} = \mathbf{x}_m + \tilde{\mathbf{x}}_{imp_s}$, $\dot{\mathbf{x}}_{imp_s} = \dot{\mathbf{x}}_m + \dot{\tilde{\mathbf{x}}}_{imp_s}$, and $\ddot{\mathbf{x}}_{imp_s} = \ddot{\mathbf{x}}_m + \ddot{\tilde{\mathbf{x}}}_{imp_s}$. Since a direct measurement of the master robot acceleration is challenging, it is estimated as

$$\ddot{\mathbf{x}}_{m_{est}} \simeq \frac{1}{m_m}(\mathbf{f}_h - k_{\mathrm{f}}\mathbf{f}_e) - \frac{c_m}{m_m}\dot{\mathbf{x}}_m - \frac{k_m}{m_m}(\mathbf{x}_m - \mathbf{x}_0) \tag{9}$$

Equations (7) and (8) can be rewrite using Property 3, the linear parameterization

$$\mathbf{f}_m = \hat{\mathbf{M}}_{\mathbf{x},m}(-\lambda_{1,m}\mathbf{s}_m + \ddot{\mathbf{x}}_{r,m}) + \hat{\mathbf{C}}_{\mathbf{x},m}\dot{\mathbf{x}}_{r,m} + \hat{\mathbf{G}}_{\mathbf{x},m} + \hat{\mathbf{F}}_{\mathbf{x},m} - \mathbf{f}_{sur} = \mathbf{Y}_{\mathbf{x},m}\hat{\boldsymbol{\theta}}_{\mathbf{x},m} - \mathbf{f}_{sur} \tag{10}$$

$$\mathbf{f}_s = \hat{\mathbf{M}}_{\mathbf{x},s}(-\lambda_{1,s}\mathbf{s}_s + \ddot{\mathbf{x}}_{r,s}) + \hat{\mathbf{C}}_{\mathbf{x},s}\dot{\mathbf{x}}_{r,s} + \hat{\mathbf{G}}_{\mathbf{x},s} + \hat{\mathbf{F}}_{\mathbf{x},s} + \mathbf{f}_{env} = \mathbf{Y}_{\mathbf{x},s}\hat{\boldsymbol{\theta}}_{\mathbf{x},s} + \mathbf{f}_{env} \tag{11}$$

The closed-loop dynamics of the master and slave robots using the above bilateral adaptive impedance controller are expressed as

$$\mathbf{M}_{\mathbf{x},m}(\dot{\mathbf{s}}_m + \lambda_{1,m}\mathbf{s}_m) + \mathbf{C}_{\mathbf{x},m}\mathbf{s}_m = \mathbf{Y}_{\mathbf{x},m}\tilde{\boldsymbol{\theta}}_{\mathbf{x},m} \tag{12}$$

$$\mathbf{M}_{\mathbf{x},s}(\mathbf{s}_s + \lambda_{1,s}\,\mathbf{s}_s) + \mathbf{C}_{\mathbf{x},s}\mathbf{s}_s = \mathbf{Y}_{\mathbf{x},s}\tilde{\boldsymbol{\theta}}_{\mathbf{x},s} \tag{13}$$

where $\tilde{\boldsymbol{\theta}}_{\mathbf{x},i} = \hat{\boldsymbol{\theta}}_{\mathbf{x},i} - \boldsymbol{\theta}_{\mathbf{x},i}$ is the estimation error of robot dynamic parameter vector.

To further proof the stability of the system and the tracking convergence of the robots' trajectories, a positive definite Lyapunov function candidate is used

$$\mathbf{V}(t) = \frac{1}{2}\left(\mathbf{s}_m^T\mathbf{M}_{\mathbf{x},m}\mathbf{s}_m + \tilde{\boldsymbol{\theta}}_{\mathbf{x},m}^T\mathbf{W}_m^{-1}\tilde{\boldsymbol{\theta}}_{\mathbf{x},m} + \mathbf{s}_s^T\mathbf{M}_{\mathbf{x},s}\mathbf{s}_s + \tilde{\boldsymbol{\theta}}_{\mathbf{x},s}^T\mathbf{W}_s^{-1}\tilde{\boldsymbol{\theta}}_{\mathbf{x},s}\right) \tag{14}$$

where $\mathbf{M}_{\mathbf{x},i}$ and $\mathbf{W}_i$ are positive definite matrices.

On the basis of the second property of robot dynamics, and by combining (12), (13) with (14), the time derivative of $\mathbf{V}(t)$ is obtained as

$$\dot{\mathbf{V}}(t) = \left(-\lambda_{1,m}\mathbf{s}_m^T\mathbf{M}_{\mathbf{x},m}\mathbf{s}_m - \lambda_{1,s}\mathbf{s}_s^T\mathbf{M}_{\mathbf{x},s}\mathbf{s}_s\right) + \left(\mathbf{s}_m^T\mathbf{Y}_{\mathbf{x},m}\tilde{\boldsymbol{\theta}}_{\mathbf{x},m} + \dot{\tilde{\boldsymbol{\theta}}}_{\mathbf{x},m}^T\mathbf{W}_m^{-1}\tilde{\boldsymbol{\theta}}_{\mathbf{x},m} + \mathbf{s}_s^T\mathbf{Y}_{\mathbf{x},s}\tilde{\boldsymbol{\theta}}_{\mathbf{x},s} + \dot{\tilde{\boldsymbol{\theta}}}_{\mathbf{x},s}^T\mathbf{W}_s^{-1}\tilde{\boldsymbol{\theta}}_{\mathbf{x},s}\right) \tag{15}$$

The adaptation laws for updating the estimated parameters of the system are defined as

$$\dot{\tilde{\boldsymbol{\theta}}}_{\mathbf{x},m} = -\mathbf{W}_m^T\,\mathbf{Y}_{\mathbf{x},m}^T\mathbf{s}_m^T\,,\ \dot{\tilde{\boldsymbol{\theta}}}_{\mathbf{x},s} = -\mathbf{W}_s^T\,\mathbf{Y}_{\mathbf{x},s}^T\mathbf{s}_s^T \tag{16}$$

Then, $\dot{\mathbf{V}}(t)$ can be simplified to

$$\dot{\mathbf{V}}(t) = -\lambda_{1,m}\mathbf{s}_m^T\mathbf{M}_{\mathbf{x},m}\mathbf{s}_m - \lambda_{1,s}\mathbf{s}_s^T\mathbf{M}_{\mathbf{x},s}\mathbf{s}_s \le 0 \tag{17}$$

The second order time derivative of $\mathbf{V}(t)$ is found as

$$\ddot{\mathbf{V}}(t) = -\lambda_{1,m}\mathbf{s}_m^T\dot{\mathbf{M}}_{\mathbf{x},m}\mathbf{s}_m - 2\lambda_{1,m}\mathbf{s}_m^T\mathbf{M}_{\mathbf{x},m}\dot{\mathbf{s}}_m - \lambda_{1,s}\mathbf{s}_s^T\dot{\mathbf{M}}_{\mathbf{x},s}\mathbf{s}_s - 2\lambda_{1,s}\mathbf{s}_s^T\mathbf{M}_{\mathbf{x},s}\dot{\mathbf{s}}_s \tag{18}$$

As $\mathbf{s}_i$, $\dot{\mathbf{s}}_i$, $\mathbf{M}_{\mathbf{x},i}$, and $\dot{\mathbf{M}}_{\mathbf{x},i}$ are all bounded, thus $\ddot{\mathbf{V}}(t)$ is bounded. Using Barbalat's lemma [22], it is proved that $\mathbf{s}_i \to 0$ and consequently $\tilde{\mathbf{x}}_i \to 0$ ($\mathbf{x}_i \to \mathbf{x}_{imp_i}$) as $t \to \infty$. As a result, the control strategy makes the system stable and ensures the master and slave robots track the corresponding impedance models' responses.

The parameters used in the control laws and the adaptation laws are shown in TABLE 2 based on experimental adjustment.

TABLE 2 PARAMETERS OF THE CONTROL LAWS AND ADAPTATION LAWS

Control Laws	Adaptation Laws
$\lambda_{1,m} = 50, \lambda_{2,m} = 0.14$	$\mathbf{W}_m = 2\mathbf{I}$
$\lambda_{1,s} = 420, \lambda_{2,s} = 0.14$	$\mathbf{W}_s = 32\mathbf{I}$

3. EXPERIMENTS AND RESULTS

In this section, the experimental setup and the experimental user study are described. This user study was approved by the University of Alberta's Research Ethics Office as Reference No. Pro00055825 – Measuring User Performance in Controlling a Robot Through a User Interface.

3.1. Experimental Setup

The experimental setup employs a Phantom Premium 1.5A robot (Geomagic Inc., Wilmington, MA, USA) with three DOFs as the master robot and a Quanser planar robot (Quanser Consulting Inc., Markham, ON, Canada) with two DOFs as the slave robot (Fig. 4(a)). To measure the applied interaction forces of the surgeon and the heart tissue, the Phantom Premium and Quanser robots are respectively equipped with a 6-axis 50M31 force/torque sensor (JR3

Inc., Woodland, CA, USA) and a 6-axis Gamma force/torque sensor (ATI Industrial Automation, Apex, NC, USA), respectively. An ultrasound scanner (SonixTouch from Ultrasonix, Richmond, BC, Canada) is used by the operator to see the surgical tool and the simulated heart, both of which are submerged in water to represent the presence of blood inside the heart's chamber.

The red dashed box in Fig. 4(a), which is magnified in Fig. 4(b), includes a handheld anchor deployment device, a simulated moving heart tissue, a surgical tool, and the ultrasound probe (Fig. 4(b)). The anchor driver is inserted into a 16-gauge blunt needle (OD 1.651mm) and fixed on the end-effector of the slave robot. By pressing the button of the anchor driver, an anchor can be pushed out from the surgical tool tip. The heart tissue is simulated by an artificial plastisol-based tissue made of soft plastic that is visible under ultrasound. This tissue is attached to a custom-built mechanical cam which produces peak-to-peak amplitude of 9 mm and has a fundamental frequency of 64 bpm to simulate the beating-heart's motion which temporally matched to an ECG signal [25]. These instruments are placed in a tank with water. To verify the results of automated heart tissue tracking by the slave robot, real-time position measurement of the beating-heart simulator was collected from a potentiometer. The position of the ultrasound probe is adjusted such that the motions of surgical tool tip and the heart tissue are both visible to the surgeon (Fig. 5).

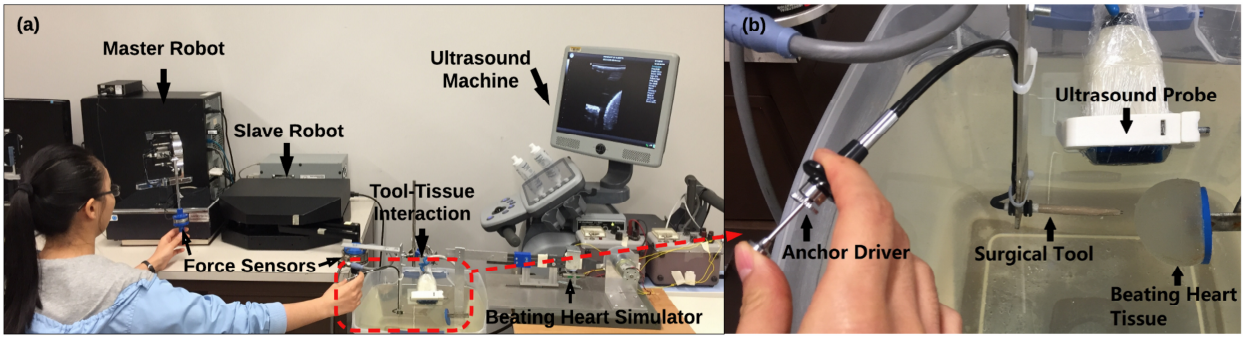

Fig.4. **Experimental setup: (a) master, slave and heart simulator, and (b) tool-tissue interaction.**

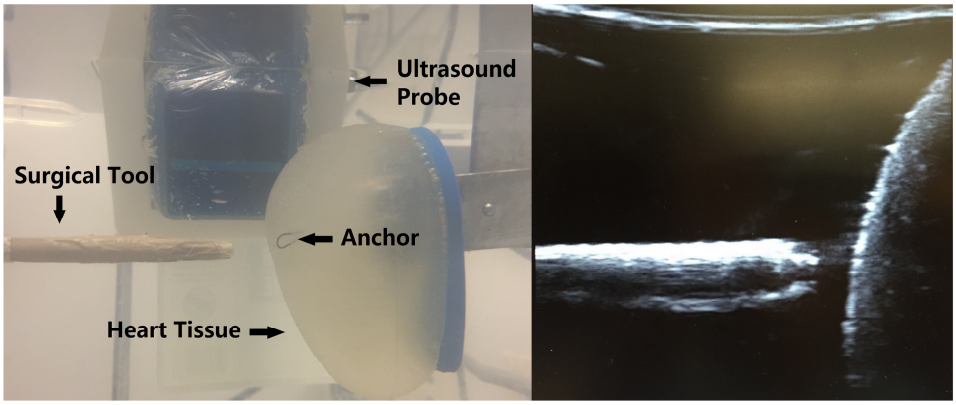

Fig.5. **(a) Underwater view of the surgical tool and heart tissue, and (b) their ultrasound image.**

3.2. Experimental Protocol

We had 8 participants (4 males and 4 females) deploy anchors into the moving heart tissue under the guidance of ultrasound images with and without robotic motion compensation. All of the participants who were not surgeons ages 22-32. Specifically, the former condition uses the proposed bilateral adaptive controller, and the latter uses a

regular direct force reflection teleoperation controller [26], which reflects the entire slave-heart tissue contact force to the master robot and requires the surgeon to take care of the motion compensation manually.

For a successful anchor deployment task, each participant should insert the anchor into the heart tissue firmly to a depth of at least 5 mm (the length of anchor is 10 mm). Moreover, as safety is a very important consideration when using robots in beating-heart surgery, in order to not harm the heart tissue, the anchor deployment forces should not exceed 2 N [20]. When the deployment force is greater than 2 N, the trial will be treated as a failure.

The experiments include two steps: training and test. To begin, each participant was allowed to deploy anchors three times with motion compensation. Then, they practiced to repeat the task without motion compensation until they got used to the device. After that, 10 trials with and without motion compensation were completed by each participant.

For each participant and each trial, several performance metrics are calculated (TABLE 3). Here, it should be noted that the contact duration is defined as the time when the slave-heart tissue interaction force is greater than 0.4 N. Also, three time-related metrics are considered: synchronization time, stapling time, and total completion time. During tool-tissue contact, a mean absolute synchronization error can be calculated to reflect the tissue deformation and motion compensation accuracy. Another important metric is the maximum force applied by the operator. A related key matric is the maximum force applied on tissue, which directly reflects the risk of tissue injury. Based on this force, the excess force rate can be obtained. The success rate is calculated to reflect both successful anchor deployment and non-excessive force application.

TABLE 3 PERFORMANCE METRICS

Performance Metric	Related to	Description	Function
Synchronization Time	Trial	The time from the beginning to the contact start	Viability and complexity
Stapling Time	Trial	The time from the contact start to stapling	
Total Completion Time	Trial	The sum of synchronization time and stapling time for a trial	
Mean Absolute Synchronization Error	Trial	$\mathrm{MAPE} = \frac{1}{n}\sum_{i=1}^{n}\lvert e_i \rvert$, where e_i is the position error between surgical tool tip and the heart tissue, n is the samples number of contact duration	Tissue deformation and motion compensation accuracy
Maximum Force by Operator On Master	Trial	The maximum force of operator applied on the master during the contact	Complexity
Maximum Force by Slave on Tissue	Trial	The maximum slave/heart interaction force during the contact	Safety of the system
Excess Force Rate	Operator	The rate of anchor deployment force being greater that 2 N	Safety of the device-tissue interaction instrument
Anchor Deployment Rate	Operator	The rate of deploying anchors with a depth greater than 5 mm	Anchor deployment accuracy
Success Rate	Operator	The rate of successfully deploying anchors while applying forces less than 2 N on tissue	Success rate of the anchor deployment system

3.3. Experimental Results

The results of performance metrics are listed in TABLE 4 with respect to two cases (with and without motion compensation). To compare the results of the two cases, a paired two-sided t-test [27] was used to obtain the

probability of the null hypothesis for the trials under different conditions as each participant performed two trials for cases with motion compensation and without motion compensation. A p-value of less than 0.05 was considered statistically significant.

TABLE 4 EXPERIMENTAL RESULTS

Robot-assisted motion compensation		**Yes**	**No**	**P-value**
Time	Synchronization Time (s)	8.32±2.68	11.34±2.90	0.0041
	Stapling Time (s)	5.94±2.12	7.58±3.49	0.0824
	Total Completion Time (s)	14.26±2.00	18.92±5.81	0.0019
Position and Force	Mean Absolute Synchronization Error (mm)	1.73±0.32	2.42±1.67	0.0151
	Maximum Force by Operator on Master (N)	1.03±0.35	1.54±0.78	0.0004
	Maximum Force by Slave on Tissue (N)	1.38±0.34	1.60±0.67	0.0313
Rate	Excess Force Rate (%)	7.5±10.35	25±25.63	0.0875
	Anchor Deployment Rate (%)	92.5±10.35	60±18.52	0.0034
	Success Rate (%)	85±9.26	42.5±16.69	0.0011

3.3.1. Operating Time

With robotic stabilization, the system provided a mean instrument synchronization time that was roughly 30% less than that measured for the case of no motion compensation. The mean total completion time using the proposed motion compensation system was much less compared to the other case, and the standard deviation was reduced by 66%. A statistically significant difference between the means of total completion times was apparent using a two-sided t-test ($p = 0.0019$).

3.3.2. Position and Force Results

Providing no compensation, the mean and standard deviation of mean absolute synchronization error were 2.42 ± 1.67 mm (mean ± std. error). However, by providing motion compensation, these values were reduced to 1.73 ± 0.32 mm. The two-sided t-test shows that there was a clear difference between the two position errors ($p = 0.0151$).

Averaged across all trials, manual contact with the tissue yielded operator's maximum forces on master of 1.54 ± 0.78 N. The proposed method of impedance control reduced these to 1.03 ± 0.35 N with clear statistical significance in a two-sided t-test ($p = 0.0004$). Additionally, the two-sided t-test also shows a significant difference with respect to not providing compensation between male and female ($p = 0.0048$), but not with respect to providing compensation ($p = 0.0863$). These values present that compared to male, female participants may have been more careful and gentle in terms of manually compensating for the heart motion with reductions of mean and standard deviation by 35% and 46%, respectively (male = 1.86 ± 0.89 N, female = 1.21 ± 0.48 N).

The maximum force by slave on tissue in each trial for each participant was recorded (see Fig. 6(a)). The excess force rate for each participant was presented in Fig. 6(b). Motion compensated anchor driving provided a mean excess force rate that was roughly 70% less than that observed without motion compensation. When providing motion compensation, there was no significant difference between male and female with respect to the maximum force by slave on tissue ($p = 0.8464$). However, providing no compensation, there was a statistically significant difference with a probability of 0.0042 (male = 1.89 ± 0.73 N, female = 1.32 ± 0.48 N).

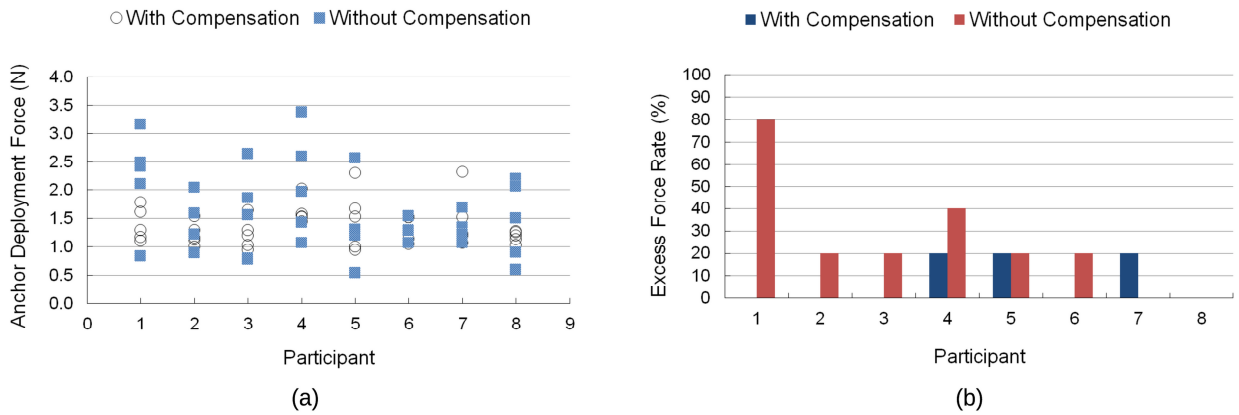

Fig.6. **The maximum force on tissue: (a) the maximum forces applied on tissue of each trial for each participant, and (b) the excess force rate for each participant.**

For the case of no motion compensation, the oscillatory interaction force of slave-heart tissue will be directly reflected to the master robot, which means once the contact occurs, the operator feels the whole haptic feedback coming from the moving tissue. For this case, there are two tricks can be used to complete the surgery. Operator 1 tried to apply large forces to the master robot during the contact, which introduced large interaction forces, small amplitudes of slave robot's position, and big tissue deformations (Fig. 7(a)). Another trick for the operator was manually compensating the motion of the beating simulator, which operator could be realized by attempting to move the master robot back and forth synchronously with the tissue (Fig. 7(b)). Comparatively, Fig. 8 shows the results of interaction forces and positions with motion compensation.

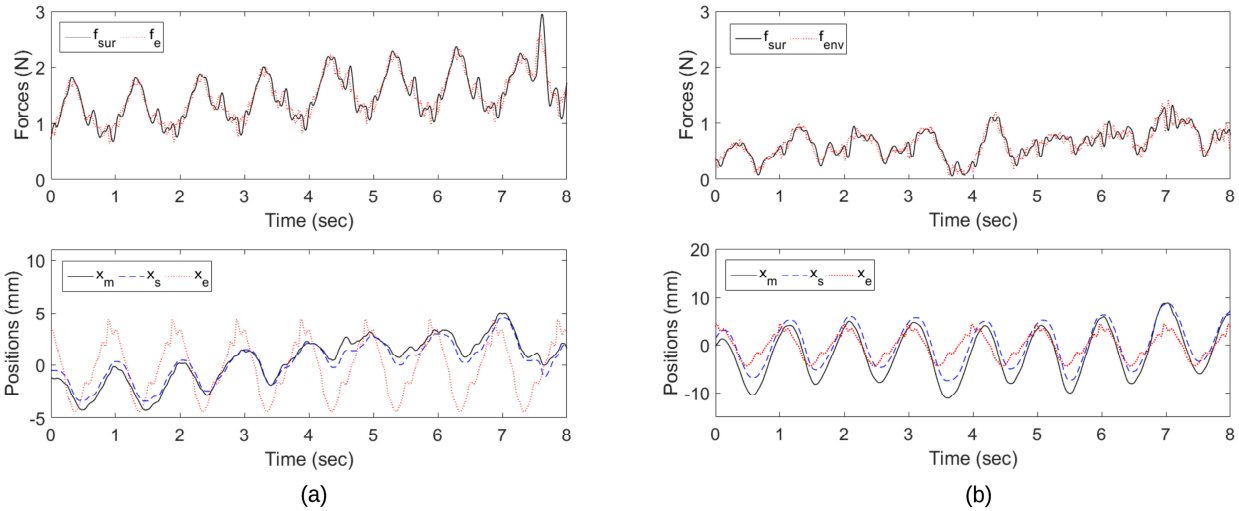

Fig.7. **Contact forces and positions under no motion compensation (a) when the operator applies a large force, and (b) when the operator applies a small force. f_{sur} (upper solid line) is the operator-master interaction force, f_{env} (upper dotted line) is the slave-heart interaction force, x_m (below solid line) is the position of the master robot, x_s (below dashed line) is the position of the slave robot, x_e (below dotted line) is the position of the heart tissue.**

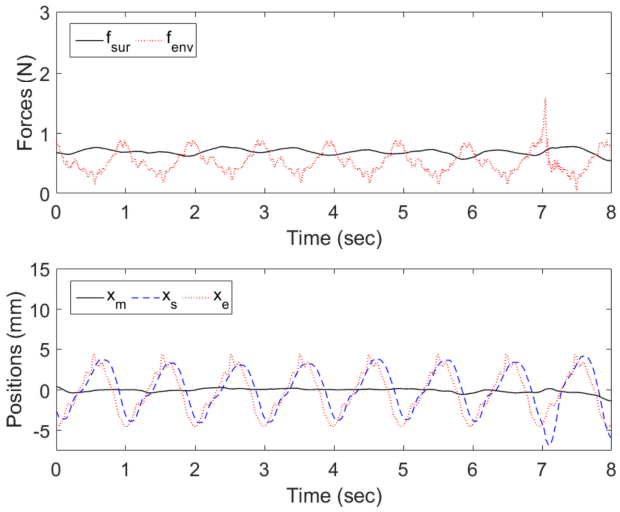

Fig.8. Contact forces and positions with the motion compensation.

3.3.3. Excess Force Rate and Success Rate

With motion compensation, the anchor deployment rate was 92.5% and the excess force rate was 7.5% of the trials, yielding the final success rate of anchor deployment to be 85%. Without compensation, the anchor deployment rate was 60% and the excess force rate was 25%, and the final success rate of anchor deployment reduced to 42.5%. The anchor deployment rate and success rate are given in Fig. 9. The t-test p-value, 0.0011, promises a statistically significant difference between the means of success rates.

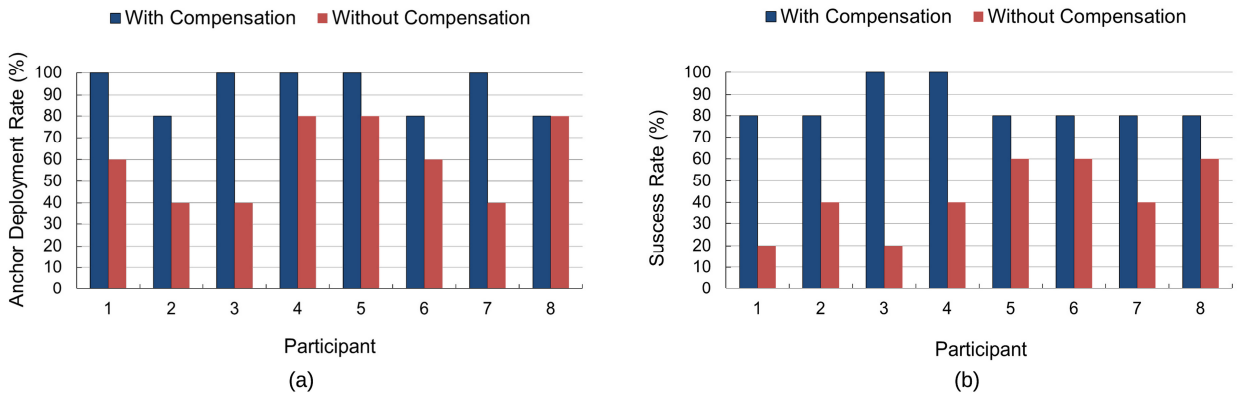

Fig.9. The anchor deployment rate and the success rate for each participant: (a) the anchor deployment rate, and (b) the success rates considering the excessive force.

In addition, a two-sided t-test was used again to compare the success rates for male and female, and the result shows that there was not a significant difference with respect to the success rate with compensation ($p = 0.1817$), but there was with respect to the case of without compensation ($p = 0.0154$).

4. DISCUSSIONS

Results from the study of operating time demonstrate that using the proposed robotic motion compensation system the participant can be much faster to adapt the heart's rapid motion and do the anchor deployment task so that

decrease the possibility of operator's fatigue during the procedure. Reduced possibility of tool-tissue collision and tissue injury was achieved when providing motion compensation by comparing the maximum forces applied on tissue under two cases. Fig. 6 (a) shows that the forces with motion compensation are generally smaller and more consistent compared to those without compensation, which means that the maximum force by slave on tissue is much easier to be controlled and kept within 2 N when providing motion compensation.

Providing no motion compensation, some operators applied large forces to hold the master robot relatively firmly (Fig. 7 (a)), but obviously the risk of tissue injury would be very high, and the position and force metrics would be large as well. Some others tried to manually compensate the motion of the beating simulator to decrease the possibility of excessive interaction force (Fig. 7 (b)), but it would also reduce the success rate of anchor deployment as the contact was not tight enough. Moreover, by manually making compensation, the operator needs more time to complete the task and it is much easier to be exhausted. The two tricks imply a trade-off between the high success rate and the safety of surgery. Without motion compensation, the operator needed to pay more attention on the forces applied to the master robot, causing the procedure to become time-consuming, high-risk, and with low success rate.

When the surgical tool contacted the tissue under motion compensation case, the oscillatory force of the moving tissue was filtered and only a stable baseline contact force was reflected to the operator (Fig. 8). To control the surgical tool tip to perform an accurate motion tracking and improve the success rate of anchor deployment, the operator could just apply a small stable force to the master robot to keep the surgical tool in a tight contact with the tissue surface. The small position deviation between the surgical tool tip and the tissue during this tight contact was caused by the tissue deformation. Generally, with compensation, the operator was more easily able to perform the task, and the interaction forces were more likely to be kept within 2 N as the force and position of the operator were all non-oscillatory.

In all of the force control experiments, the operator expressed greater confidence in instrument manipulation on the beating mitral annulus, making the impedance controller also subjectively better than the regular direct force reflection teleoperation controller. These findings suggest that the stabilization of the force reflected to the operator is an effective aid to the operator for beating heart mitral annuloplasty.

Additionally, there is another interesting result should be noted that the motion compensation strategy has an advantage in terms of reducing the significant difference between the male and female with respect to the applied maximum forces by slave on tissue and the success rate of anchor deployment. One possible reason is that maybe the female operator is more scrupulous and better at controlling forces when there is motion compensation.

Previous research has shown that motion tracking of intracardiac beating-heart tissue by surgical robot is feasible [28-30]. However, much of these work used a hand-held device for surgery instead of utilizing a teleoperation system, which poses additional challenges due to the dynamical interferences of the master and slave robot (i.e., any lack of "transparency" of the master-slave teleoperation system makes motion compensation and robot operation harder than the case where the master and the slave are unified to one hand-held device). Moreover, the above ultrasound image-based methods would result in an accurate motion tracking of the heart tissue by the surgical robot as long as the surgical tool tip and the heart tissue did not make contact. During interactions with the surgical tool, the tissue deformation makes it difficult to extract the tool and tissue position based on ultrasound images.

For this reason, other researchers have proposed methods using force control to implement motion compensation [31-33]. Hara et al. [34] and Kempf et al. [35] showed that repetitive control methods based on force are well suited for quasi-periodic servoing tasks. Ginhoux et al. [36] and Bebek and Cavusoglu [37] successively proposed using a force-based model predictive controller to improve motion tracking accuracy. While the tracking performances are good, past work did not incorporate haptic feedback to the surgeon. Kitagawa et al. show that with the addition of force feedback, both accuracy and repeatability of the forces improve [32]. Moreover, force feedback would help to decrease tissue damages and prevent undesirable trauma [38].

In our proposed strategy, the system we developed can not only feedback the non-oscillatory slave-heart tissue interaction force to the surgeon but also make compensation for the rapid heart's motion. This system does not need the sensor for the tool-tissue interaction force to be placed inside the body. It also does not require any heart motion prediction, observation and/or learning, making it easy to implement. Nevertheless, there are still a number of

aspects to be improved. Future work may involve extending the motion compensation technology to multi-DOF cardiac surgeries and exploring the system's potential uses in other forms of beating heart procedure that may require complex tissue trajectory tracking, such as pericardiectomy, myocardial injury suture, catheter ablation, and so on. In addition, the fixed parameters of the impedance models during the experiments can be designed to be variable to increase the robustness of the system.

5. CONCLUSION

This paper has demonstrated the viability and superiority of a bilateral impedance-controlled telerobotic system performing beating-heart anchor deployment for mitral valve annuloplasty under the guidance of ultrasound images. This system has been shown reduce operation time, increase safety to the heart tissue, achieve lower and more stable force application by the operator, and obtain high success rate of deploying anchors. The telerobotic system with an anchor driver attached to the slave robot's end-effector reduced the excess force application rate by 70%, and increased the success rate of anchor deployment by 100% compared to manual attempts. The motion compensation instrument also decreased the task completion time (from the operation start to stapling) by 22% and reduced the mean absolute synchronization error by 30%. Low and stable operator forces were achieved when compared to the case of without compensation.

ACKNOWLEDGEMENTS

This work is supported by the Canada Foundation for Innovation (CFI) under grant LOF 28241， the Alberta Innovation and Advanced Education Ministry under Small Equipment Grant RCP-12-021, the Natural Sciences and Engineering Research Council (NSERC) of Canada under grant RGPIN 372042, the Natural Sciences and Engineering Research Council (NSERC) of Canada under grant RGPIN 03907, and the China Scholarship Council (CSC) under grant [2015]08410152.

REFERENCES

[1] Greer AD, Newhook PM, and Sutherland GR. Human-machine interface for robotic surgery and stereotaxy. *IEEE/ASME Transactions on Mechatronics*. 2008; 13(3): 355-361.
[2] Burgner J, Rucher DC, Gilbert HB, *et al*. A telerobotic system for transnasal surgery. *IEEE/ASME Transactions on Mechatronics*. 2014; 19(3): 996-1006.
[3] Ruszkowski A, Mohareri O, Lichtenstein S, *et al*. On the feasibility of heart motion compensation on the daVinci® surgical robot for coronary artery bypass surgery: Implementation and user studies. In *Proceedings of the IEEE International Conference on Robotics and Automation*. Seattle, WA, USA; 2015; p. 4432-4439.
[4] Dacey LJ, Likosky DS, Leavitt BJ, *et al*. Perioperative stroke and long-term survival after coronary bypass graft surgery. *The Annals of Thoracic Surgery.* 2005; 79(2): 532-537.
[5] Newman MF, Kirchner JL, Phillips-Bute B, *et al*. Longitudinal assessment of neurocognitive function after coronary-artery bypass surgery. *New England Journal of Medicine*. 2001; 344: 395-402.
[6] Paparella D, Yau TM, and Young E. Cardiopulmonary bypass induced inflammation: pathophysiology and treatment. An update. *European Journal Cardio-Thoracic Surgery*. 2002; 21: 232-244.
[7] Zeitlhofer J, Asenbaum S, Spiss C, *et al*. Central nervous system function after cardiopulmonary bypass. *European Heart Journal*. 1993; 14: 885-890.
[8] Bellinger DC, Wypij D, Kuban KCK, *et al*. Developmental and neurological status of children at 4 years of age after heart surgery with hypothermic circulatory arrest or low-flow cardiopulmonary bypass. *Circulation*. 1999; 100: 526-532.
[9] Angelini GD, Taylor FC, Reeves BC, Ascione R. Early and midterm outcome after off-pump and on-pump surgery in beating heart against cardioplegic arrest studies (BHACAS 1 and 2): a pooled analysis of two randomised controlled trials. *Lancet.* 2002; 359: 1194-1199.
[10] Fix J, Isada L, Cosgrove D, *et al*. Do patients with less than 'echo-perfect' results from mitral valve repair by intraoperative echocardiography have a different outcome? *Circulation*. 1993; 88 (suppl II): II39-48.

[11] Nakamura Y, Kishi K, and Kawakami H. Heartbeat synchronization for robotic cardiac surgery. In *Proceedings of the IEEE International Conference on Robotics and Automation*. Seoul, South Korea; 2001; p. 2014-2019.
[12] Ginhoux R, Gangloff J, De Mathelin M, *et al*. Active filtering of physiological motion in robotized surgery using predictive control. *IEEE Transactions on Robotics.* 2005; 21(1): 67-79.
[13] Bowthorpe M, Tavakoli M, Becher H, Howe R. Smith predictor based robot control for ultrasound-guided teleoperated beating-heart surgery. *IEEE Journal of Biomedical and Health Informatics*. 2014; 18(1): 157-166.
[14] Bowthorpe M and Tavakoli M. Ultrasound-based image guidance and motion compensation control for robot-assisted beating-heart surgery. *Journal of Medical Robotics Research*. 2016; 1(1): 1640002(11 pages).
[15] Bowthorpe M and Tavakoli M. Generalized predictive control of a surgical robot for beating-heart surgery under delayed and slowly-sampled ultrasound image data. *IEEE Robotics and Automation Letters.* 2016; 1(2): 892-899.
[16] Bonow RO, Carabello BA, Kanu C,, *et al*. ACC/AHA 2006 guidelines for the management of patients with valvular heart disease: a report of the American College of Cardiology/American Heart Association Task Force on Practice Guidelines (writing committee to revise the 1998 Guidelines for the Management of Patients With Valvular Heart Disease): developed in collaboration with the Society of Cardiovascular Anesthesiologists: endorsed by the Society for Cardiovascular Angiography and Interventions and the Society of Thoracic Surgeons. *Circulation.* 2006; 114: e84-e231.
[17] De Oliveira JMF and Antunes MJ. Mitral valve repair: better than replacement. *Heart*. 2006; 92(2): 275-281.
[18] Rausch MK, Bothe W, Kvitting JPE, *et al*. Mitral Valve Annuloplasty: A quantitative clinical and mechanical comparison of different annuloplasty devices. *Annals of Biomedical Engineering.* 2013; 40(3): 750-761.
[19] Glower DD. Surgical approaches to mitral regurgitation. *Journal of the American College of Cardiology*. 2012; 60(15): 1315-1322.
[20] Yuen SG, Kettler DT, Howe RD, *et al*. Robotic motion compensation for beating heart intracardiac surgery. *The International Journal of Robotics Research.* 2009; 28(10): 1355-1372.
[21] Sharifi M, Salarieh H, Behzadipour S, Tavakoli M. Tele-echography of moving organs using an impedance-controlled telerobotic system. *Mechatronics (A Journal of IFAC)*. 2017; 67: 52-63.
[22] Slotine JJE and Li W. *Applied Nonlinear Control*. Englewood Cliffs, NJ: Prantice-Hall; 1991.
[23] Liu X, Tao R, Tavakoli M. Adaptive control of uncertain nonlinear teleoperation systems. *Mechatronics*. 2014; 24: 66-78.
[24] Sharifi M, Behzadipour S, and Salarieh H. Nonlinear bilateral adaptive impedance control with applications in telesurgery and telerehabilitation. *ASME Journal of Dynamic Systems, Measurement, and Control*. 2016; 138(11): 111010 (16 pages).
[25] Bowthorpe M, Castonguay-Siu V, Tavakoli M. Development of a robotic system to enable beating-heart surgery. *Journal of the Robotics Society of Japan.* 2014; 32(4): 23-30.
[26] Chiaverini S, Siciliano B, and Villani L. Force/position regulation of compliant robot manipulators. *IEEE Transactions on Automatic Control*. 1994; 39(3): 647-652.
[27] Snedecor GE and Cochran WG. The Two-tailed T-Test. *In Statistical Methods* (The lowa State University Press Ames). 1967; 59-60.
[28] Kesner SB, Howe RD. Position control of motion compensation cardiac catheters. *IEEE Transactions on Robotics*. 2011; 27(6): 1045-1055.
[29] Yuen SG, Vasilyev NV, del Nido PJ, Howe RD. Robotic tissue tracking for beating heart mitral valve surgery. *Medical Image Analysis*. 2013; 17(8): 1236-1242.
[30] Kettler DT, Plowes RD, Howe RD, *et al*. An active motion compensation instrument for beating heart mitral valve surgery. In *proceedings of the IEEE/RSJ International Conference on Intelligent Robots and Systems*. San Diego, CA, USA; 2007; p. 1290-1295.
[31] Okamura AM. Methods for haptic feedback in teleoperated robot-assisted surgery. *Industrial Robot: An International Journal.* 2004; 31: 499-508.
[32] Kitagawa M, Okamura AM, Baumgartner WA, *et al*. Analysis of suture manipulation forces for teleoperation with force feedback. In *Proceedings of the 5th International Conference on Medical Image Computing and Computer-Assisted Intervention.* Tokyo, Japan; 2002; p. 155-162.
[33] Wagner CR, Stylopoulos N, Jackson PG, and Howe RD. The benefit of force feedback in surgery: examination of blunt dissection. *Presence Teleoperators Virtual Environ.* 2007; 16(3): 252-262.
[34] Hara S, Yamamoto Y, Omata T, and Nakano M. Repetitive control system: A new type servo system for periodic exogenous signals.pdf. *IEEE Transaction on Automatic Control*. 1988; 33(7): 659-668.
[35] Kempf C, Tomizuka M, Horowitz R, and Messner W. Comparison of four discrete-time repetitive control algorithms. *IEEE Control Systems*. 1993; 13(6): 48-54.
[36] Ginhoux R, Gangloff JA, Marescaux J, *et al*. Beating heart tracking in robotic surgery using 500 Hz visual servoing, model predictive control and an adaptive observer. In *Proceedings of the IEEE International Conference on Robotics and Automation*. New Orleans, LA, UAS; 2004; p. 274-279.
[37] Bebek O and Cavusoglu MC. Model based control algorithms for robotic assisted beating heart surgery. In *Proceedings of the 28th Annual International Conference on Engineering in Medicine and Biology Society*. New York, NY, USA; 2006; p. 823–828.

[38] Tavakoli M, Aziminejad A, Patel RV, Moallem M. High-fidelity bilateral teleoperation systems and the effect of multimodal haptics. *IEEE Transactions on Systems, Man, and Cybernetics - Part B*. 2007; 37(6): 1512-1528.